Est. 1984

ORIENTAL JOURNAL OF CHEMISTRY
An International Open Free Access, Peer Reviewed Research Journal

www.orientjchem.org

ISSN: 0970-020 X
CODEN: OJCHEG
2014, Vol. 30, No. (2):
Pg. 451-461

Activated Carbon Prepared from Orange Peels Coated with Titanium Oxide Nanoparticles: Characterization and Applications in the Decomposition of NO_x

LILIANA GIRALDO[1] and JUAN CARLOS MORENO-PIRAJAN[2]*

[1]Universidad Nacional de Colombia, Facultad de Ciencias, Departamento de Química, Carrera 30 No 43-00, Bogotá, Cundinamarca, 001/Colombia
[2]*Universidad de los Andes, Facultad de Ciencias, Departamento de Química, Grupo de Investigación en Sólidos Porosos y Calorimetría, Carrera 1 No 18 A 10, Bogotá, Cundinamarca, 001/Colombia
*Corresponding author: E-mail: jumoreno@uniandes.edu.co

http://dx.doi.org/10.13005/ojc/300207

(Received: February 28, 2014; Accepted: March 30, 2014)

ABSTRACT

In this work, we report the degradation of NO_x using two catalysts prepared by coating activated carbon from orange peels with TiO_2. This study compared the performance of TiO_2-coated catalysts prepared by CVD ($AC1/TiO_2$) and the sol-gel method ($AC2/TiO_2$). The catalysts were characterized by X-ray diffraction, BET surface area and TEM. The photocatalytic activity was measured by studying the degradation of NO_x in the vapor phase. The results show that the catalyst synthesized by the CVD method was more efficient in the decomposition of NO_x. TEM and XRD revealed the presence of a mixture of the anatase and rutile phases, which favors the NO_x decomposition process. Nitrogen isotherms showed that coating the nanoparticles with titanium oxide did not significantly change the surface area of the original activated carbon.

Key words: photocatalysis, activated carbon, isotherms, NO_x degradation

INTRODUCTION

Research on pollutants and their sources that are emitted to the environment are very varied. The scientists must propose solutions to this problematic, which is an topic that today is a problem of great importance to society, problem that requires researchers with new ideas for propose the realization of solutions to the pollution control and ensure that ecosystems reach its natural balance. The research in the laboratories of the Universities have the fundamental idea that later can be applied to small-scale and large-scale later. Thus, it may in a short period of time, that the large part of the pollutants which are now environmentally hazardous, begin to decrease. Automotive traffic exhaust contains many hazardous gaseous pollutants, such as nitrogen oxides (NO_x), which

affect the health of people living in urban areas[1,2]. Reducing NO_x concentrations is therefore important in order to promote sustainable development[3,4]. The oxides of nitrogen, NO and NO_2 (NO_x), have a variety of negative impacts on human and environmental health, ranging from serving as key precursors of the respiratory irritant ozone to forming nitric acid, which is a key component of acid rain. Hence, it is of great interest to develop approaches that irreversibly remove NO_x from the atmosphere.

Industrial development in the past five decades has brought the planet to a very worrying collapse from the environmental point of view because of the uncontrolled increase in the use of fossil fuels as the main energy source; the average global temperature will increase and thereby alter the ecosystem. In particular, the excess emission of gases from the internal combustion engine and industry has become one of the major causes of environmental pollution, where gases such as CO_2, CO, hydrocarbons, SO_2, and NO_x generate volatile organic compounds (VOC) and particulate matter. These compounds have led to the greenhouse effect, acid rain, photochemical smog, stratospheric ozone depletion, and the aforementioned global warming. These events impose considerable negative effects on human and animal health due to the high toxicity of the compounds mentioned[1,2]. Nitrogen compounds such as nitrogen oxides (NO_x) and sulfur (SO_x), which are considered the most toxic gases, are emitted into the atmosphere during the combustion of fossil fuels. To reduce these emissions, several studies have used porous materials such as mesoporous materials, modified mesoporous materials, aluminas, silicon compounds, compounds derived from coal as both chemically and physically activated powders, granular materials, and fabrics modified with TiO_2[5,6]. Nitrogen oxide (NO_x) emissions into the atmosphere have a direct impact on the global environment and human health through ozone depletion, photochemical smog and acid deposition[1-3]. The wet scrubbing method is an efûcient and economical way to remove soluble pollutants[3]. In order to remove NO_x by the wet scrubbing method, it is necessary to oxidize nitric oxide (NO) into the more soluble nitrogen dioxide (NO_2) or dinitrogen pentoxide (N_2O_5) in either the gas or liquid phase[4-9]. However, it is very difûcult to oxidize dilute NO without the addition of strong oxidants such as methanol, ozone and hydrogen peroxide[5–10].

For several decades, it has been known that heterogeneous photocatalysis represents an emerging environmental control option for the efficient removal of chemical pollutants, as it can be applied to water and air purification. This process involves a nano-solid semiconductor catalyst, usually titanium dioxide (TiO_2), which is activated with ultraviolet light at the appropriate wavelength. For various reasons, titanium dioxide in the anatase form has been the preferred choice due to its strong oxidizing power under UV irradiation, its chemical stability and the absence of toxicity[11]. These reactions are very attractive for treating pollution because: (1) in the vast majority of cases pollutants are transformed into innocuous products[11,12] and (2) the process has very low selectivity, thus permitting the treatment of a wide range of contaminants. Nowadays, smog is still problematic. Researchers have dedicated their time to studying the dynamics of the photocatalysis of nitrogen oxides. While some have focused on NO_x control methodology by the reduction to NO_x to N_2[11,13], another approach is to oxidize NO to NO_2 and HNO_3 along the general direction of nitrogen fixation. Photocatalytic oxidation (PCO) of NO_x offers the following important advantages: (1) no extra reactants are required and (2) NO_x is recycled or recovered as nitric acid, a potential raw material for fertilizers. The scientific literature has reported a number of interesting publications on the treatment of NO_x with TiO_2, so photodegradation for this compound. There are also interesting publications in which kinetic studies have been carried out on the possible mechanisms of the TiO_2 photocatalytic reaction with NOx[11,17]. Several researchers[11,14] have discovered that, during the photodegradation process, interaction with certain pollutant molecules or their intermediates can cause the TiO_2 powder to coagulate, thereby reducing the amount of UV radiation able to reach TiO_2 active centers (due to a reduction in surface area), thus reducing its catalytic effectiveness[11]. In order to overcome this coagulation problem, some researchers have used different materials as a support for the titania photocatalyst. Various substrates have been used as a catalyst support for the photocatalytic degradation of polluted water. From a survey of the literature, we can

establish certain criteria for selecting an optimal catalyst support. The supporting material should be transparent or at least allow some UV radiation to pass through it and be chemically inert or non-reactive to pollutant molecules, its intermediates and the surrounding aqueous system. The supporting material should sufficiently bond either via physically or chemically to TiO_2 without reducing the reactivity of titania. The supporting material should have a high surface area and a strong adsorption affinity for the pollutants (organic or inorganic compounds) to be degraded. This criterion reduces or eliminates the intermediates produced during the photocatalytic degradation while further increasing mass transfer rates and processes for efficient photodegradation. The supporting material should also allow for fast and easy photocatalyst recovery and re-use with or without regeneration. Based on these criteria, activated carbon (AC) has been extensively researched and used as a support material for TiO_2[11,16,17].

Besides being used as a catalyst support, some researchers have used TiO_2 and AC mixtures to treat pollutants. The literature reports some benefits of AC supports in the preparation of titania photocatalysts. A greater AC content in the supported photocatalyst translates to a higher surface area for the supported photocatalyst and higher adsorption capacity. The pore volume of AC is directly proportionate to the amount of AC in the catalyst[11], indicating that TiO_2 particles actually agglomerate on the carbon surface without being adsorbed into the carbon pores. However, pore trapping may still occur to a small extent. An AC content less than 13% of the supported photocatalyst weight will create a homogeneous distribution of TiO_2 on the surface[11,18]. A heterogeneous distribution will occur if the percentage of the carbon is greater than 13%, causing both the AC and TiO_2 particles to form conglomerates. Organic compounds are hydrophobic, whereas TiO_2 particles, when exposed to UV radiation, are hydrophilic. Using AC as a photocatalyst support will help bring the pollutant molecules closer to the TiO_2 active site (to come in contact with hydroxyl radicals) for an efficient and effective photodegradation process (synergistic effect). AC can generate new adsorption centers to favor approaching pollutant molecules. Using activated carbon as a support will also enable secondary degradation of intermediates to take place in situ, further enhancing the effectiveness of the photocatalyst. Moreover, using AC as a support allows for fast and easy photocatalyst recovery and provides ample room for catalyst regeneration using various techniques[11-16,18]. This is because the supported photocatalyst can be made into a granular form, providing an easy filtering option for recovery from the slurry[11]. Besides possessing all the criteria and benefits of a catalyst support as established in the literature survey, AC is non-polar, non-reactive, highly adsorptive and cheap to manufacture or purchase.

The purpose of the present work was to prepare AC from orange peel under specific conditions in the lab and to deposit on its surface nanoparticles of TiO_2 using two different techniques, with the purpose of comparing its performance in the decomposition efficiency of NO_x.

Methods and Experimental

Materials

AC was prepared as reported in our previously published work[19]. Prior to use, the orange peel was repeatedly washed with distilled water in order to remove dust and other inorganic impurities, then oven-dried for 24 h at 393 K to reduce the moisture content and milled to a size < 1 mm. Peels from Colombian oranges were impregnated with an aqueous solution of KOH following a variant of the incipient wetness method; similar cases have been described in the literature[19-27]. This consists of adding dropwise (while stirring the solid, to facilitate homogeneous absorption of the liquid) a specific amount of the aqueous solution (2.0 mL g^{-1} orange peel) necessary to produce swelling until incipient wetness. In this study, the concentration of KOH in the aqueous solution was 160 wt%, which was expressed as the impregnation ratio (X_p, wt.%), defined as (g KOH per g orange peel)×100. After impregnation, the samples were dried for 8 h at 383 K in air. Pyrolysis treatment (activation) was carried out in a vertical tubular reactor made of quartz in a Carbolite™ furnace, in all cases using 25 g of the impregnated and dried material. All treatments were performed at a constant heating rate of 10 K min^{-1} and with an argon (99.999% pure)

flow of 30 STP $cm^3.min^{-1}$, which was maintained during heating and cooling. An activation temperature of 823 K and a soaking time of 4 h were used. After cooling the solid pyrolysis residue to room temperature, it was washed with Milli-Q distilled water until the conductivity of the washing liquid was lowered to <5 ¼S cm^{-1} (measured using a pH/conductivity meter; HP, model MARK 602). The resulting ACs was dried at 383 K for 24 h in a vacuum furnace.

Preparation of the photocatalyst samples

Chemical vapor deposition (CVD) method

This experiment was based on the work of Ding *et al*.[28] and Amjad *et al*.[29]. We have designed and built a system based on publications by other authors by making some adjustments to improve the variability of the equipment.

The reactor for CVD synthesis consisted of a quartz tube that was made of this material due to its chemical inertia during the evaporation of the reagent, which was inserted into a tubular furnace in order to obtain the desired coating temperature. As the particles of the support were quite small and as there was no means to support them, we designed and adapted a porous glass plate for the final part of the reactor that holds the activated carbon during the reaction and promoting the free passage of vapors. Seven milliliters of titanium tetra iso-propoxide (TTIP) were placed in flask (a) of the reactor, while another container (b) was kept empty and immersed in an ice bath. The containers (a) and (b) were heated using two adjacent boiling water baths, which were heated before placing flasks (a) and (b), and kept under an inert atmosphere of nitrogen gas flowing through the system at a 1.7 L/min. This flow rate was sufficient to cause continuous movement of the particles inside the second flask to ensure homogeneity. When all the TTIP was consumed, water baths were switched off and the nitrogen flow was kept on until the system reached room temperature. The sample was then washed three times with distilled water to remove any suspended undeposited titanium hydroxide. The sample was then dried at 150°C overnight, then calcined for 3 h at 600°C to produce the anatase form of titanium dioxide. This procedure was followed has been reported in the literature[28,29]. This sample was designated AC1/TiO_2.

Sol–gel impregnation method

A nano-sized binary mixed oxide of AC/TiO_2 was prepared by the sol–gel impregnation method[30]. The synthetic procedure followed a typical sol–gel impregnation method to prepare a 1:1 molar composition of AC/Ti mixed oxide. Under constant magnetic stirring, 7.6 mL of titanium tetraisopropoxide were added dropwise to a beaker containing 25 mL of isopropanol and 1.5 mL HCl, while the beaker was maintained at 0°C. In another beaker, 8.2 mg of AC were suspended in 25 mL of isopropanol and then was mixed dropwise into the first beaker with vigorous stirring. The mixture was then stirred at 25°C for 48 h. The mixed sol was then sonicated in an ultrasonicator (up 200 s, Hielscher, Germany) at room temperature for 30 min. The sonicated sol was placed over a hotplate to remove the solvent. The resulting powder was calcined at a specific temperature and time. Nano-sized titanium dioxide was prepared using a similar approach.

Under constant magnetic stirring, 7.6 mL of titanium tetraisopropoxide were added dropwise to a beaker containing 25 mL of a solvent such as isopropanol and 1.5 mL HCl, an the temperature of beaker was kept at 0°C using a water and ice bath. The mixture was stirred at 25°C for 48 h. The resulting sol was then sonicated for 30 min and then the solvent was removed over a hotplate with a rather slow stirring rate. The powder was calcined at the desired temperature and time. This simple was designated AC2/TiO_2.

Textural characterization of activated carbons and the prepared catalysts

To determine the surface area and pore structure of activated carbon samples, the nitrogen adsorption–desorption isotherms at 77 K were measured by an automated adsorption instrument (IQ2 Quantachrome, Boynton Beach, FL, USA) with ± 0.15% accuracy. The surface area, pore volume and pore size distribution were determined from nitrogen adsorption data using Quantachrome software. Adsorption data were obtained over the relative pressure, P/P^o, range from 10^{-5} to 1. The sample was degassed at 250°C under a vacuum for 4 h. The apparent surface area of nitrogen was calculated using the BET (Brunauer–Emmett–Teller) equation within the 0.01–0.3 relative pressure range. The micropore volume was determined according

to the DR (Dubinin–Radushkevich) method[31-34]. The amount of N_2 adsorbed at relative pressures near unity (~0.99) corresponds to the total amount adsorbed in both micropores and mesopores; consequently, the subtraction of the micropore volume from the total amount will provide the volume of the mesopores. The pore size distribution was obtained by applying the density functional theory (DFT) method to the nitrogen adsorption isotherm using the software supplied by IQ2[31-32].

Catalyst characterization

X-ray powder diffraction (XRD)

XRD was performed using a Rigaku MiniFlex-II X-ray diffractometer with Cu Kα radiation (λ=0.15418 nm). The sample was scanned from 20° to 80° (2¸) at a rate of 0.02°/min. The phases present in the catalyst samples were identified using the Joint Committee on Powder Diffraction Standard (JCPDS) powder data files. The XRD pattern and data were also analyzed using the Powder X program[35-39]. From these XRD patterns, the crystallite or grain size (d_{XRD}) of the prepared powders was estimated using the Scherrer equation (Eq.1) as follows[10,33-35]:

$$d_{XRD} = K \times \lambda / \beta \times \cos\theta \quad ...(1)$$

where λ, θ and β are the X-ray wavelength, Bragg diffraction angle and the full width at half-maximum (FWHM) of the diffraction peak, respectively. K is a constant normally equal to 0.94 and λ=0.1540 nm (the wavelength of emission of the device).

Transmission electron microscopy

TEM measurements were performed on a Philips G20 Ultra-Twin transmission electron microscope equipped with a CCD camera. Operating at 300 kV, the microscope can achieve a point resolution of 0.14 nm and a line resolution of 0.1 nm. Scale calibration was done on the Au (1 0 0) planes. Both dry and wet deposition were performed with ethanol and water as the solvents. Powders were deposited on carbon coated copper grids.

Photocatalytic activity measurements: reactor and test

Fig. 1 depicts the continuous flow system used for NO_x degradation over AC1/TiO_2 and AC2/TiO_2. A round Pyrex glass vessel (φ× H, 15 cm × 4 cm) was used as the photoreactor to assess the degradation of NO_x, and a sample dish (φ 7 cm) was located inside the vessel containing the nanoparticles of TiO_2 supported on AC. A black lamp provided a UV light source with an intensity of 1 mW/cm^2 (Sankyo Denki FL 20SBLB, main peak located at 352 nm). NO_x degradation was carried out at room temperature using an air stream containing 1.0 ppm NO as the feedstock. Two mass flow controllers (MFCs) (type MFC-CB control box, Fluka, USA) manipulated the relative humidity (RH = 50%) in the feeding stream. The reaction gas in the feeding stream passed through a vessel containing TiO_2 supported on AC (0.2 g) at a flow rate of 1 L/min. The measurements of NO and NO_x concentrations were performed using an on-line chemiluminescence analyzer (AC32M, Environnement SA, France) with a detection limit of 0.4 ppb and a continuous sampling rate of 0.7 L/min. NO and NO_x concentrations were measured in successive 5-s steps. The NO_2 concentration was obtained from the difference between the NO_x and NO concentrations[12,36].

Fig. 1: Schematic diagram of the continuous flow reaction system for the photocatalytic degradation of NO: 1. Mass flow controler 2.Tramp 3. Peristaltic pump 4. Chemiluminescence equipment 5. UV source 6.Reactor 7. Computer

RESULTS

Specific surface area and pore structural characterization analysis of the activated carbon

The N_2 adsorption isotherms at 77 K of both the untreated sample (AC without titanium oxide) and samples coated with titanium oxide are shown in Fig. 2. The adsorption isotherms of the activated

carbons exhibited a hybrid I/IV isotherm according to the IUPAC classification, which is characteristic of microporous materials with an important contribution of mesoporosity[37]. The N_2 adsorption isotherms also showed a hysteresis loop (type H4) at relative pressures about 0.5 where the adsorption and desorption branches were parallel; this indicates the presence of small slit-shaped pores and well-developed mesoporosity for all the catalysts[37]. Isotherm data were analyzed for BET area, total pore volume, micropore volume and average pore width. Specific surface areas were calculated according to the BET method. Total pore volumes were directly derived from the adsorbed quantity at high relative pressures (P/P^o 0.95, where P^o is the saturation pressure of nitrogen at 77.36 K and equals 101.38 kPa). The results obtained from the nitrogen isotherms are presented in Table 1. Adsorption data were analyzed by the NLDFT equilibrium model for slit pores and the pore size distributions (PSD) were calculated[38]. The PSD, i.e. the distribution of pore volume with respect to pore size, is represented by the derivative of dV/dr as a function of r, where V is the pore volume and r is the pore radius. In the case of carbons, in which the pores are considered to be mostly slit-shaped, pore width (w) can replace pore radius (r), and the PSD can be presented similarly by the derivative of dV/dw as a function of w (results not shown).

When the AC was coated with titanium oxide using the CVD and sol-gel methods, the porous structure was modified. This change in the textural structure was most noticeable in the AC2/TiO_2 sample. This can be explained considering that, in this catalyst, particles may plug some of the pores, whereas the AC covered using the CVD method had a greater number of particles in the pores because a TiO_2 vapor was generated. This type of change was observed in the values of the apparent BET area and PSD. These results are consistent, and it was found that the pore size was smaller for AC2/TiO_2, as suggested in the previous paragraph.

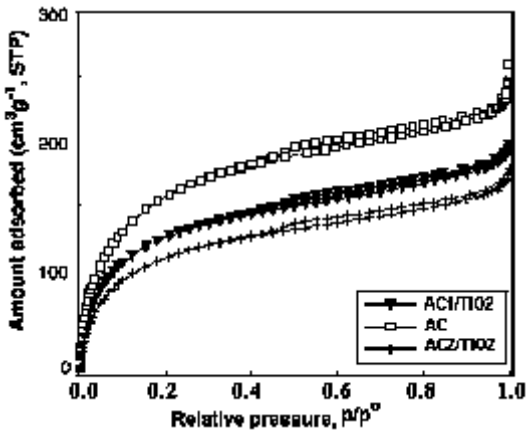

Fig. 2: N_2 adsorption isotherms at 77 K for the activated carbons prepared from orange peel (AC, AC1/TiO_2 and AC2/TiO_2)

XRD analysis

The materials were analyzed by XRD and the results are shown in Fig. 3. The diffraction patterns of pure TiO_2, AC alone, AC1/TiO_2, and AC2/TiO_2 are presented for comparison. The two broad peaks of the AC prepared from orange peel sample indicate that the content of the well-ordered crystalline phase can be neglected. The peak from 20° to 30° 2¸ corresponds to reflexes in the (002) plane, whereas the peak from 40° to 48° 2¸ corresponds to the (100) plane[39-42]. The pattern exhibits broad peaks and the absence of a sharp peak indicating a predominantly amorphous structure, which is a typical characteristic of AC. This also indicates an advantageous property for well-defined adsorbents.

The photocatalysts were dominated mainly by the anatase phase. The main diffraction peaks at 25.3°, 37.8°, 48°, 53.9°, 55° and 62.5° 2¸ were assigned to the diffraction planes of (1 0 1), (0 0 4), (2 0 0), (1 0 5), (2 1 1) and (2 0 4) for anatase (JCPDS # 021-1272), respectively. Other crystal phases corresponding to peaks at 27.4 and 36.1° 2¸ were assigned the diffraction peaks of (1 1 0) and (1 0 1) of the rutile phase (JCPDS # 021-1276), respectively. The XRD patterns revealed the diffraction peaks of a mixture of the anatase and rutile phases, which is favorable for photocatalytic reactions[43-49]. XRD also showed that the AC prepared in this study did not affect the crystal structure of TiO_2 when it was deposited on AC by the CVD method, but the peak intensity was lower and the peaks were wider, while the peaks in the AC2/TiO_2 samples decreased and some cases were barely visible. This clearly shows the influence of the method used to coat AC with titanium oxide. Data analysis of the XRD patterns was performed

using the PowderX program. The crystallite or grain size (d_{XRD}) was determined using the Scherrer formula. The anatase (compound principal registered) crystallite sizes of AC1/TiO_2 and AC2/TiO_2 were 3.4 and 4.5 nm, respectively. The diffraction peak width increased with increasing BET surface area and pore volume, as shown above. Therefore, the crystal size of TiO_2 decreased according to Eq. (1). This is in agreement with the literature on nanostructured powders with high purity[44-49]. The method used to coat AC with TiO_2 may be responsible for this reduction in crystallite size, because the formation of TiO_2 in the CVD method, which is performed in the vapor phase, allows free particles to enter the pores of AC, while the sol-gel method produces small agglomerations of particles with a slightly larger size.

This suggests that AC could enhance the photocatalytic activity of NO_x and would be presented in composited samples in this case with TiO_2. Furthermore, in additional calculations, the anatase content ($f_{(A)}$) was determined from the integrated intensity of the anatase diffraction line (1 0 1), IA, and that of the rutile diffraction line (1 1 0), IR, using the following equation (Eq. 2)[46].

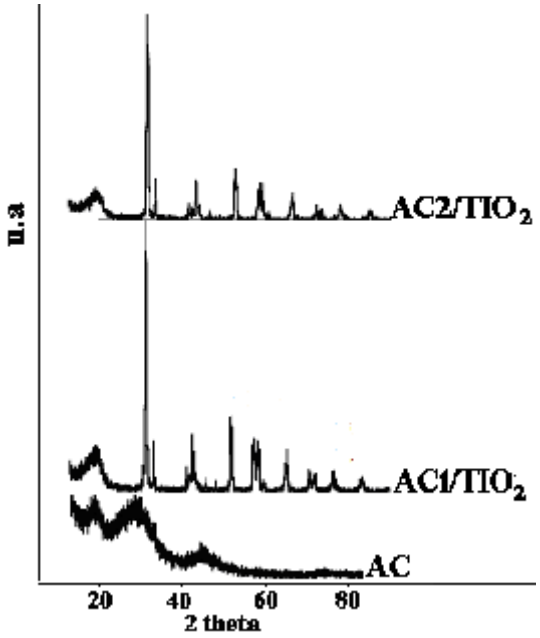

Fig. 3: XRD patterns of the prepared samples

$$f_{(A)} = \frac{1}{1+12.6\frac{I_A}{I_R}} \quad ...(2)$$

The anatase content of AC1/TiO_2 and AC2/TiO_2 was 0.977 and 0.898, respectively. The $f_{(A)}$ values show that the phases of the obtained catalysts were mainly anatase with a small amount of rutile.

TEM analysis

Fig. 4 shows TEM images of the AC1/TiO_2 and AC2/TiO_2 samples. The samples clearly present a microstructure consisting of TiO_2 nanoparticles (H"3 nm) homogeneously dispersed on AC, especially in the case of AC1/TiO_2. After coating, the titanium oxide nanoparticles remain homogeneously dispersed around the porous structure of AC (Fig. 4a).

The AC1/TiO_2 sample (Fig. 4a) showed TiO_2 nanoparticles embedded on a mass of AC obtained from orange peel. The image indicates that there were effective interactions between the oxide and the chemical groups on the carbon, as result of the more efficient CVD preparation method developed in this work. This corroborates the XRD results, which indicated that TiO_2 particles penetrated the more porous structure of AC when the CVD method was used. Fig. 4b show a TEM image of the AC2/TiO_2 sample, with accumulation of quite visible particles, unlike those obtained by the CVD method.

NO_x degradation results

Before starting the photocatalytic experiment, we performed several preliminary studies to optimize several variables such gas flow, temperature and other variables for the catalytic test of the photoactivity of the AC1/TiO_2 and AC2/TiO_2 systems in the NO_x degradation reaction, as described in the Experimental section. The NO and NO_2 concentrations were monitored continuously, and a profile of the concentrations as a function time was recorded (see Fig. 5 for a representative plot). As expected, the pure AC pure was catalytically inactive in the reaction, while the AC1/TiO_2 and AC2/TiO_2 catalysts were active under our experimental conditions and showed good

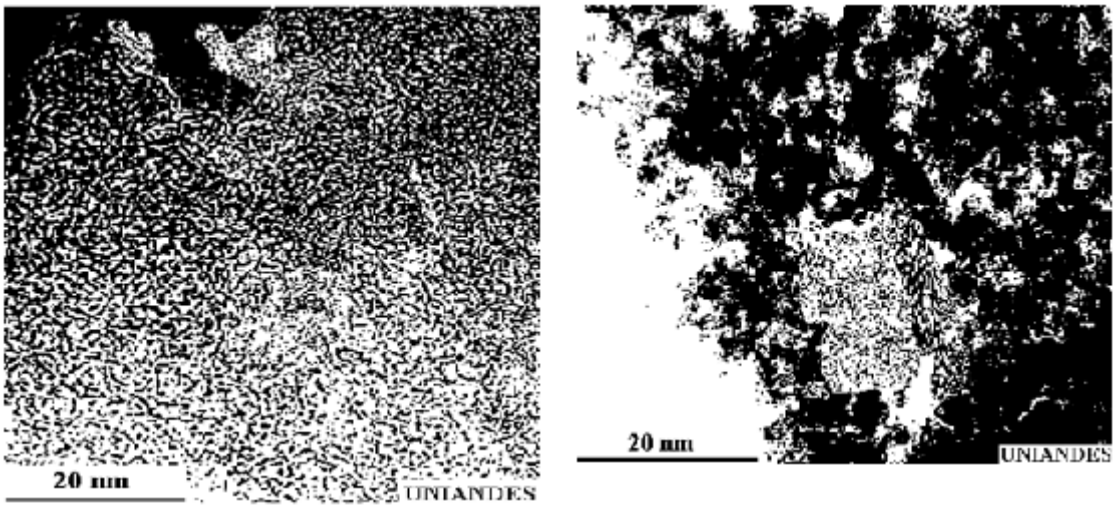

Fig. 4: TEM photographs of (a) AC1/TiO_2 and (b) AC2/TiO_2

conversion values. As shown in Fig. 5, the NO concentration reached a minimum value followed by a slow and continuous deactivation process after the adsorption of NO_3^- on the catalytic active sites. Simple adsorption and desorption of NO gas (not due to photocatalysis) by the catalysts (AC1/TiO_2 and AC2/TiO_2) occurred in the dark (Fig. 5(a) and (b)). The net removal of NO gas at the beginning of illumination for AC1/TiO_2 was higher in comparison to AC2/TiO_2 The results show that the conversion values were associated with the TiO_2 coating method, since the catalytic activity of AC1/TiO_2 was greater than that of AC2/TiO_2; this was associated with the findings described earlier. The sample obtained by the CVD method had higher catalytic activity, which shows that the deposited vapor phase TiO_2 was more efficient than TiO_2 deposition by the sol-gel method where the pores of the AC were blocked. The CVD method allows for the uniform deposition of TiO_2nanoparticles within the porous structure, which generates a more active sample. Fig. 5 shows the typical evolution of the NO, NO_x and NO_2 concentrations during a test intended to assess the photocatalytic efficiency of the coating. The degradation of nitrogen oxides by photocatalysis led to the oxidation of NO to NO_2, which, in turn, produced nitrite and nitrate ions (reaction (4)).

The mechanism of the photocatalytic reaction using supported nanoparticles of titanium, in this case AC prepared from orange peel, has been studied by several authors and is published in the literature[50,51]. Several studies agree on a number of steps that we reproduced in our research, considering that these reactions are very consistent with what we have established in this investigation. Thus, we believe that the photocatalytic process occurs in three main steps: (1) mass transport and adsorption of pollutants from the bulk air to the

Table 1 : Structural parameters calculated from nitrogen adsorption isotherms at 77 K for the samples prepared in this research

Sample	S_{BET}[$m^2.g^{-1}$]	V_{TOTAL}[$cm^3.g^{-1}$]	V_{MICRO}[$cm^3.g^{-1}$][a]	V_{MESO}[$cm^3.g^{-1}$][b]	W_o, N_2(DR)[$cm^3.g^{-1}$]
AC	625	0.55	0.33	0.12	0.32
AC1/TiO_2	580	0.50	0.30	0.10	0.28
AC2/TiO_2	500	0.45	0.26	0.07	0.24

[a] Evaluated at P/P^o H~0.95. [b] Evaluated from DFT applied to N_2 adsorption data.

surface of the catalyst; (2) photocatalytic reaction on the catalyst; (3) desorption and mass transport of the reaction products from the surface of the catalyst to the air. The photocatalytic oxidation mechanism has been investigated extensively[51-55]. Based on previous publications[50,51] and the results of the present study, we believe that Eqs. (3)–(12) represent the photocatalytic reaction mechanism of NO. Eq. (3) shows the photon-mediated generation of electron/hole pairs[50-52].

$$TiO_2 + h\mu \rightarrow ||e^+ + h^- \quad ...(3)$$

Eqs. (2)-(4) show the adsorption of the reactants onto the photocatalyst:

$$TiO_2 + H_2O \rightarrow TiO_2\_H_2O \quad ...(4)$$

$$TiO_2 + O_2 \rightarrow |TiO_2\_O_2 \quad ...(5)$$

$$TiO_2 + NO \rightarrow TiO_2\_NO \quad ...(6)$$

Eq.(5) shows the recombination of the generated electron and hole pairs:

$$e^- + h^+ \rightarrow \text{heat} \quad ...(7)$$

Eq.(5) and (7) show the trapping of the generated holes and electrons:

$$h+ + H_2O \rightarrow OH^- + H^+ \quad ...(8)$$

$$e^- + O_2 \rightarrow O_2^- \quad ...(9)$$

Eqs.(8)-(10) show the oxidation of NO:

$$NO + OH^- \rightarrow HNO_2 \quad ...(10)$$

$$HNO_2 + OH^- \rightarrow NO_2 + H_2O \quad ...(11)$$

$$NO_2 + OH^- \rightarrow NO_3^- + H^+ \quad ...(12)$$

These reactions clearly show the role of adsorbed oxygen and water and its very important role in the heterogeneous photocatalytic oxidation reaction. Oxygen is used to trap the generated electrons on the TiO_2 surface coating on AC. Hydroxyl radicals are produced from water by trapping the generated holes on the TiO_2 surface, which then leads to the oxidation of NO_2 and finally NO_3^-. In another series of studies reported in the literature, these reactions clearly show the role of oxygen and water[56].

The photocatalytic oxidation reaction takes place immediately when the sample is exposed to the visible light. The NO_2 concentration increases and quickly reaches a stable condition. After reaching the maximum degradation rate, the process will slightly slow down and reach a stable conversion condition. Fig. 3 shows the concentration change in NOx during the photocatalytic oxidation reaction. The photocatalytic oxidation of NO is calculated from Eq. (13):

$$NO_{con}(\%) = [C_{con}]_{in}\text{-}[C_{NO}]_{out}/[C_{NO}]_{in}100 \quad ...(13)$$

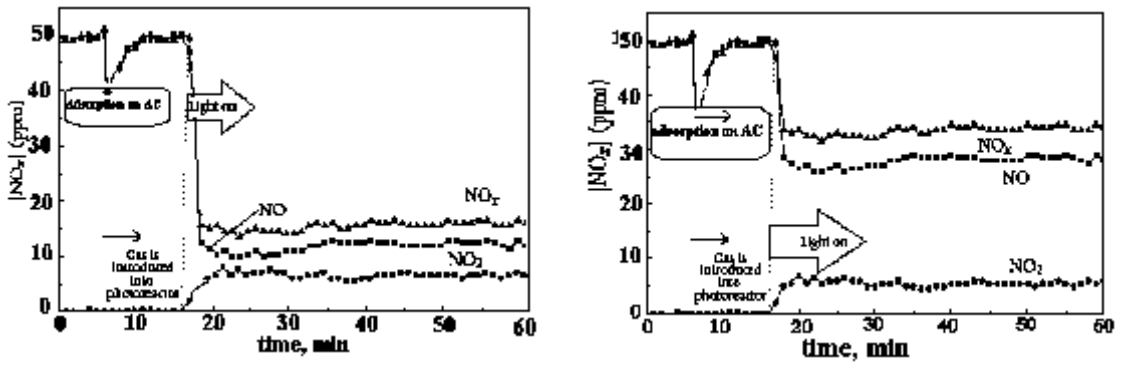

(a) $AC1/TiO_2$ (b) $AC2/TiO_2$

Fig. 5: Profiles of variation in the NO_x concentration in the reactor during a typical test

where $[C_{NO}]_{out}$ is defined as the average NO concentration of the last 5 min in the measurement time. Eq. (11) shows the formation of NO_2 during the oxidation reaction. However, not all the produced NO_2 can be oxidized to HNO_3 because a small part of it is released into the air due to desorption. So, the exit pollutant is composed of the remaining NO and the undesired intermediate NO_2. The amount of NO_x removed is calculated using Eq. (14):

$$NO_{xcon}(\%) = [C_{NOx}]_{in}\text{-}[C_{NOx}]_{out}/[C_{NOx}]_{in}100 \quad ...(14)$$

where $[C_{NOx}]_{out}$ is defined as the average NO_x concentration at the exit port in the last 5 min of the measurement time.

CONCLUSIONS

In this study, two catalysts (AC1/TiO_2 and AC2/TiO_2) were prepared using AC derived from orange peel by two different methods to achieve the deposition of titanium oxide nanoparticles (CVD and sol-gel). The results show the superiority of the AC1/TiO_2 catalyst, prepared using the CVD method to apply TiO_2 nanoparticles onto the surface of the AC, because this method allows vaporized nanoparticles to enter into the porous structure. The XRD results show that the nanoparticles were a mixture of the anatase and rutile phases, which makes the catalyst more efficient regarding NO_x degradation. NO_x degradation assays were used to test catalyst efficiency.

ACKNOWLEDGMENTS

The authors wish to thank the framework agreement between the Universidad Nacional de Colombia and the Universidad de los Andes (Colombia) under which this research was carried out. Additionally, the authors thank the Faculty of Sciences and the Vice-Rector of Research of the Universidad de los Andes (Bogotá, Colombia) for funding this research.

REFERENCES

1. Ao, C.H.; Lee, S.C.; Mak, C.L.; Chan, L.Y. *Appl. Catal. B*, **2003**, *42*,119-129
2. Haywood, J.M.; Cooper, C.D. *J. Air Waste Manage. Assoc*. **1998**, *48*, 238–246
3. Adewuyi, Y.G.; Owusu, S.O. *Ind. Eng. Chem. Res.* **2003**, *42*, 4084–4100
4. Farrell, A. *Energy Policy*, **2001**,*29*,1061–1072
5. Sekiguchi, K.; Saito, M.; Lee.Y.; Kim, Y.; Sakamoto, K. *Chem. Eng. J.* **2006**, *118*, 127–130
6. Castro, T.; Madronich, S.; Rivale, S.; Muhlia, A.; Mar, B. *Atmos. Environ.* **2001**, *35*, 1765–1772
7. Mok, Y.S. *Chem. Eng. J.* **2006**, *118*, 63–67
8. Zamansky, V.M.; Ho, L.; Maly, P.M.; Seeker, W.R. *Combust. Sci. Technol.* **1996**, *120*, 255–272
9. Ibusuki, T.; Takeuchi, K. *J. Mol. Catal.* **1994**, *88*, 93–102 (1994).
10. Wu, Z.; Sheng, Z.; Liu, Y.; Mo, H.W.J. *J. of Hazardous Mat.* **2011,** *185*, **1**053–1058
11. Monge, M.e.; D´Anna, B.; George, C. *Phys. Chem. Chem. Phys.* **2010**, *12* (31), 8991-8998
12. Ballari, M.M.; Hunger, M.; Husken, G.; Brouwers, H.J.H. *Appl. Catal. B: Env.* **2010**, *95*, 245–254
13. Puma, G.L.; Bono, A.; Krishnaiah, D.; Collin, J.G. *J. of Haz. Mat.* **2008**, *157*, 209–219
14. Matos, J.; Laine, J.; Hermann, *J. Appl. Catal. B: Environ*. **1998**, *18* (3–4), 281–291
15. Herrmann, J.; Matos, J.; Disdier, J.; Guillard, C.; Laine, J.; Malato, S.; Blanco, J. *Catal. Today*. 1999, *54 (2-3)*; 255–265 (1999).
16. Hu, Z.; Vansant, E.F. *Microp. and Mesop. Mater*. **1995**, *3(6)*, 603–612
17. Arriagada, R.; Garcia, R.; Molina-Sabio, M., Rodriguez-Reinoso, F., *Microp. and Mesop. Mater*. **1997**, *8(3–4)*, 123-130
18. Arana, J.; Dona-Rodriguez, J.M.; Rendon, E.T.; Cabo, C.G.; Gonzalez-Diaz, O.; Herrera-Melian, J.A.; Perez-Peña, J.; Colon, G.; Navio, J.A. Appl. Catal. B. **2003**, *44(2)*, 161–172
19. Moreno-Piraján, J.C.; Giraldo, L. *E-Journal of Chemistry*. **2012**, *9(2)*, 926-937
20. Keith, K. H.; McKay, G. *J. Hazard Mater.* **2008**, *160*, 845-854

21. Purevsuren, B.; Avid, B.; Narangerel, J.; Gerelmaa, T.; Davaajav, Y. *J. Mater. Sci.* **2004**, *9(2)*, 737-740
22. Hsisheng. T.; Hsieh, C.T. *Ind. Eng. Chem. Res.* **1998**, *37(9)*, 3618-3624
23. Suárez-García, F.; Martínez-Alonso, A.; Tascón, J.M.D. *Carbon*. **2001**, *39*, 1111-1115
24. Molina-Sabio, M.; Rodríguez-Reinoso, F.; Caturla, F.; Sellés, J.M. Carbon, 1995, *33*, 1105-1113
25. Baquero M C, Giraldo L, Moreno J.C, Suárez-García F, Martínez-Alonso, A. Tascón, J.M.D. *J Therm Anal Appl Pyrol*. **2003**, *70*, 779-784
26. Moreno-Piraján, J.C.; Giraldo, L., *J. Anal Appl Pyrol.* **2010**, *87(2)*, 288-290
27. Moreno-Piraján, J.C.; Giraldo, L. *J. Anal Appl Pyrol*. **2010**, *87(2)*, 188-193
28. Ding, Z.; Hu, X.; Yue, P.; Lu, G.; Greenfield, P. *Cat.Today.* **2001**, *68*, 173-182
29. Amjad, H.; El-Sheikh, A. P.; Newman, H.A.D.; Suki, P.; Neil, C.; Steven, Y. *Surf. & Coat. Tech.* **2004**, *187*, 284– 292
30. Slimena, H.; Houasa, A.; Nogierb, J.P. *J. of Phot.y and Photobio. A: Chem.* **2001**, *221*, 13–21
31. Stoeckli, F.; Centeno, T.A.; Donnet, J.B.; Pusset, N.; Papirer, E. *Fuel.* **1995**, *74*, 1582-88
32. Nakagawa, Y.; Molina-Sabio, M.; Rodríguez-Reinoso, F. *Micropor. Mesopor. Mat*, 2007, *103*, 29-34
33. Yorgun, S.; Vural, N.; Demiral, H. *Micropor. Mesopor. Mater.* **2009**, 122, 189–194
34. Vargas-Delgadillo, D.; Giraldo, L.; Moreno-Piraján, J.C. *E-Journal. Chem*. **2010**, *7*, 531-539
35. Hirano, M.; Nakahara, C.; Ota, K.; Tanaike, O.; Inagaki, M. *J. Solid State Chem.* **2003**, *170*, 39–47
36. Dalton, J.S.; Janes, P.A.; Jones, N.G.; Nicholson, J.A.; Hallam, K.R.; Allen, G.C. *Env. Poll.* **2002**, *120*, 415–422
37. Sing, K.S.W.; Everett, D.H.; Haul, R.A.W.; Moscou, L.; Pierotti, R.A.; Rouquerol, J.; Siemieniewska, T. *Pure and Applied Chemistry.* **1985**, *57*, 603–619
38. Landers, J.; Gor, G.Y.; Neimark, A.V. Colloids and Surfaces A: *Physicochem. Eng. Aspects.* **2013***, 437*, 3-32
39. Linh, L.L.T.; Chin, S.; Ju, J.; Anh, H. *Powder Technology.* **2012**, *225*,167**–**175
40. Yoon, K.H.; Noh, J.S.; Kwon, C.H.; Muhammed, M. *Mat. Chem. and Phys.* **2006**, *95*, 79-83
41. Kumar, K.; Saxena, R.K.; Kothari, R.D.; Suri, K.; Kaushik, N.K.; Bohra, J.N. *Carbon*. **1997**, *35(12),*1842–1844
42. Hashemian, S.; Zahra, K.; Yazdi, A. *J. Ind. and Eng. Chem*., **2014**, *20*, 1892-1900
43. Vasilyeva, E.; Tolochko, O.; Kim, B.; Lee, D.; Kim, D. *Microelec. Jour*. **2009**, *40*, 687–691
44. Kim, J.; Kim, B. *Scripta Materialia* **2004**, *50*, 969–972
45. Wang, Z.; Choi, C.; Kim, J.; Kim, B.; Zhang, Z. *Materials Letters* **2003**, *57*, 3560–3564
46. Toyoda, M.; Nanbu, Y.; Nakazawa, Y.; Hirano, M.; Inagaki, M. *App. Cat.B: Env.* **2004,** *49*, 227–232
47. Arbuj, S.S.; Hawaldar, R.R.; Mulik, U.P.; Wani, B.N.; Amalnerkar, D.P.; Waghmode, S.B. *Mat. Sci.and Eng.B.* **2010**,*168*, 90–94
48. Spurr, R.A.; Myers, H. *Anal. Chem*. **1957**, *29*, 760–762
49. Mädler, L.; Stark, W.J.; Pratsinis, S.E. *J. of Mat. Res.* **2002***, 16*, 1356–1362
50. Yu, Q.L.; Brouwers, H.J.H. App. Cat. B: Env. **2009**, *92*, 454–461
51. Choi, J.; Park, H.; Hoffmann, M. R. *J. Mater. Res.* **2010**, *25*,149-158
52. Devahasdin, S.; Fan, C.; Li, J.K.; Chen, D.H. *J. Photochem. Photobiol. A: Chem.* **2003***, 156;* 161–170
53. Wang, H.; Wu, Z.; Zhao, W.; Guan, B. *Chemosphere.* **2007**, *66*, 185–190
54. Zhang, J.; Hu, Y.; Matsuoka, M.; Yamashita, H.; Minagawa, M.; Hidaka, H.; Anpo, M. *J. Phys. Chem. B*. **2001**, *105*, 8395–8398
55. Turchi, C.S. ; Ollis, D.F. *J. Catal.* **1990**, *122*; 178–192
56. Lim, T.H.; Jeong, S.M.; Kim, S.D.; Gyenis, J. J. Photochem. Photobiol. A: Chem. **2000**, *134*, 209–217.